Crossover from capillary fingering to viscous fingering for immiscible unstable flow: Experiment and modeling

M. Ferer,[1,2] Chuang Ji,[1,3] Grant S. Bromhal,[1] Joshua Cook,[1,3] Goodarz Ahmadi,[1,3] and Duane H. Smith[1,2]
[1]*US D.O.E., National Energy Technology Laboratory, P. O. Box 880, Morgantown, West Virginia 26507-0880, USA*
[2]*Department of Physics, West Virginia University, P. O. Box 6315, Morgantown, West Virginia 26506-6315, USA*
[3]*Department of Mechanical and Aeronautical Engineering, P. O. Box 5725, Clarkson University, Potsdam, New York 13699, USA*
(Received 21 October 2003; revised manuscript received 19 February 2004; published 8 July 2004)

Invasion percolation with trapping (IPT) and diffusion-limited aggregation (DLA) are simple fractal models, which are known to describe two-phase flow in porous media at well defined, but unphysical limits of the fluid properties and flow conditions. A decade ago, Fernandez, Rangel, and Rivero predicted a crossover from IPT (capillary fingering) to DLA (viscous fingering) for the injection of a zero-viscosity fluid as the injection velocity was increased from zero. [J. F. Fernandez, R. Rangel, and J. Rivero, Phys. Rev. Lett. **67**, 2958 (1991)]. We have performed experiments in which air is injected into a glass micromodel to displace water. These experiments clearly demonstrate this crossover as the injection velocity of the air is increased. Furthermore, simulations, using our standard pore-level model, also support the predicted IPT-to-DLA crossover, as well as the predicted power-law behavior of the characteristic crossover length.

DOI: 10.1103/PhysRevE.70.016303 PACS number(s): 47.55.Mh, 47.53.+n, 47.20.Ma

I. INTRODUCTION

The fingering of the injected fluid associated with immiscible, two-phase flow in porous media is one of the major reasons for the inefficiency of several important geologic recovery/remediation processes. In secondary oil recovery, water displaces much less than half of the oil in any given formation, because the water "fingers" into the oil-saturated reservoir. In CO_2 sequestration (a means to mitigate global warming), where carbon dioxide is injected into brine-saturated porous media (e.g., subsea floor formations, deep saline aquifers) for long-term storage, fingering limits the available storage capacity so that only a small fraction of the reservoir is occupied by CO_2. In remediation of DNAPL spills, which can enter and contaminate the ground water, standard pump and treat remediation methods are often ineffective because water flushing in porous media typically mobilizes only a small portion of the pollutant; a better understanding of the location of the DNAPL within the water table can improve this process. Our focus in all of these processes is on the efficiency of displacement, so it is important to understand how the injected fluid occupies the medium. Therefore, this study focuses on the saturation of a nonwetting fluid injected into porous media—its fingering, and its fractal character.

Two simple models of two-phase flow in porous media have been used to describe the flow in two limits which are conceptually important but seemingly unphysical: Invasion percolation with trapping (IPT) describes the flow when capillary forces are dominant (zero injection velocity), and diffusion limited aggregation (DLA) describes the flow when the injected fluid has zero viscosity and capillary forces are absent. Capillary number, a measure of the the strength of the viscous forces relative to the capillary forces, is defined as

$$N_c = \frac{\mu_d v}{\sigma \cos \theta}, \tag{1}$$

where μ_d, is the viscosity of the defending fluid, v is the injection velocity, σ is the interfacial tension, and θ is the contact angle. In a seminal 1991 paper, Fernandez and coworkers used a DLA model modified to include capillary forces to demonstrate that injection of a zero-viscosity fluid would exhibit capillary fingering (IPT behavior) for small capillary number (viscous forces $\ll$ capillary forces) and that the behavior would cross over to viscous fingering (DLA-like) as viscous forces became more important [1,2]. Furthermore, they predicted (and verified for their model) the dependence of the crossover length upon the relative strength of the capillary forces

$$\Lambda \propto (N_c)^{-2/(2+D_s)} = (N_c)^{-0.6}, \tag{2}$$

where D_s is the fractal dimension of the IPT external perimeter, i.e., $D_s = 1.33$ [3,4].

In this paper, we will test their predictions using results both from our flow cell experiments and from our standard pore-level model, which is more general than their modified DLA model [5]. The agreement of our experimental results with the predictions for the IPT-to-DLA crossover indicate that these results, which are only strictly valid at unphysical limits, i.e., $M=0$, do affect real physical behavior.

First, let us briefly review the limiting behaviors. In the first limit, zero capillary number, where capillary forces are much larger than viscous forces, Wilkinson and others introduced a simple model of immiscible, two-phase flow called invasion percolation [6,7]. In this model, the nonwetting, injected fluid advances solely through the largest throat (the one with the smallest capillary pressure) on the interface between the two fluids during each time step. Since, at small flow velocities and related pressures drops, the wetting fluid

cannot displace the nonwetting fluid, a fully encircled region of wetting fluid is immobilized or trapped, in that the nonwetting fluid is prevented from advancing into this trapped region [8]. Invasion percolation with trapping (IPT) modifies the standard IP rules to forbid advance into a "trapped" region [4,8–10]. This simple model is applicable far from an injection well, where the invasion front is becoming longer and longer so that on the interface, the local flow velocity and, therefore, the viscous forces are small. This invasion percolation model has been widely studied since its introduction [6,7,10–16]. There have also been many applications of this model and closely related models to a variety of increasingly more complex porous media flow problems [17–20]; Blunt has provided an excellent review of recent work [21]. The injection patterns have been shown to be self-similar fractals with a value of fractal dimension close to that of the standard percolation model. Recent work on large, two-dimensional systems favors a value of fractal dimension below that of ordinary critical percolation theory, $D_f \approx 1.825 \pm 0.004$, with uncertainties that exclude the ordinary critical percolation theory value, $D_f \approx 1.89$ [3,4,10,11]. Relevant to our modeling on small systems, other studies, on small systems, indicate that $D_f \approx 1.89$ is a better fit to the observed results for these system sizes [16,22–24].

In the other limit of zero capillary forces and zero-viscosity ratio,

$$M = \mu_I / \mu_d = 0 \tag{3}$$

(i.e., ratio of the viscosity of the injected fluid to that of the displaced fluid), the flow is described by diffusion-limited aggregation (DLA) [9,10,12,13,25–32]. Evidence from both experiments and modeling showed that not only were the DLA and viscous fingering patterns visually similar, but they also had the same fractal dimension [12,13,25–36]. We expect that DLA patterns on our lattices should have a fractal dimension, $D_f \approx 1.71$. For central-injection DLA on a square lattice, the clusters grown were observed to be self-similar fractals with a fractal dimension $D_f \approx 1.71$ when the clusters occupied fewer than approximately $m \approx 10^4$ lattice sites. However, as the size of the cluster increased to more than $m \approx 10^6$ lattice sites, the pattern ceased being self-similar, first becoming diamond shaped and then cross shaped with four distinct arms in the lattice directions [37]. For "off lattice" DLA mimicking real porous media that lack the symmetry axes of a lattice, the patterns are more self-similar with a fractal dimension $D_f \approx 1.70$ [38]. Since the DLA simulations on relatively small lattices produce fractal patterns (with approximately 10^4 sites) very similar to very large, off-lattice DLA patterns, we expect that our flow patterns on small diamond-lattice porous media will produce fractal patterns similar to the flow in realistically large, random porous media.

In Sec. II of this paper, we will present our experimental flow cell results. In these experiments, we have injected air into in a glass micromodel saturated with water [39]. Flow patterns from these experiments show that for this small (but nonzero) viscosity ratio, $M = 1/62.5$, small capillary number flows (small injection velocities) exhibit capillary fingering, while large capillary number (large injection velocities) flows exhibit viscous fingering. Furthermore, at moderate capillary numbers, the early time flows exhibit capillary fingering; then, as the flow patterns develop, the flows change and eventually exhibit viscous fingering.

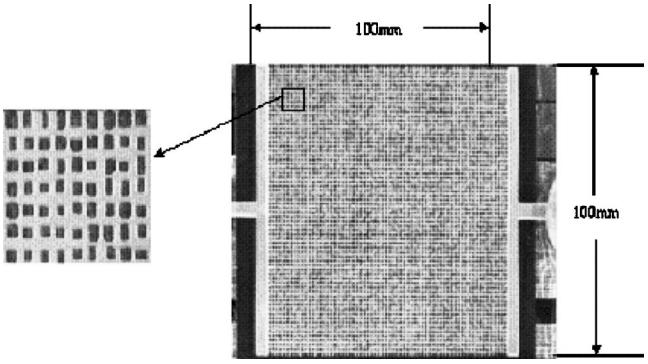

FIG. 1. Horizontal flow cell. Air is injected slowly through the inlet at the right side into a reservoir. Once the reservoir is filled, air is injected from the air-filled reservoir into the flow cell. The displaced water flows into the reservoir on the right side and then through the outlet.

In Sec. III of this paper, we present modeling results which further support these predictions and which demonstrate their relevance to real two-dimensional flows. Instead of using a DLA-based algorithm modified to account for capillary pressures, we used our standard pore-level model for a range of capillary numbers, and viscosity ratio $M = 10^{-4}$. This pore level model has been quantitatively validated in the limit of small capillary numbers and small viscosity ratios [5]. Not only do our modeling results exhibit the predicted IPT-to-DLA crossover, but they also support the predicted scaling of the crossover.

Both the experimental and modeling results show the crossover from capillary fingering (IPT-like) to viscous fingering (DLA-like) in a physical range of capillary numbers and viscosity ratios for these systems with a few thousand pore bodies (i.e., lattice sites).

II. EXPERIMENTAL FLOW CELL RESULTS

A. Experimental setup

The experimental flow cell is composed of two sheets of glass that have been fused together; one has a random, pseudo-two-dimensional matrix sandblasted into it, the other is flat; together, they form a network of randomly-sized flow channels (Fig. 1). The cell is saturated with water, and then connected to a syringe pump by 0.08 inch inner diameter nylon tubing, which controls the constant flow rate of the injected air. The process is recorded using image capture with a video camera in NTSC format (640×480), model no. 4915-4000/0000 and a Nikon Nikkor 20mm lens. The pressure applied across the cell is measured each time a picture is taken. Experiments were run over a range of flow rates. The experimental setup is shown in Fig. 2.

The flow cell, shown in Fig. 2, has an average channel width of 0.41 mm, and an average channel depth of 0.067 mm. The channel width distribution, shown in Fig. 3, is approximately uniform.

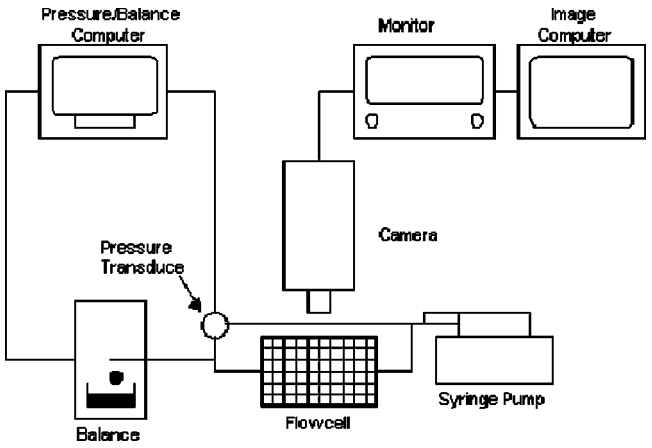

FIG. 2. Experimental setup.

Experiments were conducted by injecting air at a constant flow rate, which is controlled by the KDS 200 syringe pump. The pressure is read using a Setra C239 pressure transducer, which has a range of 0 to 30 inch water column and an output of 4–20 mA with an accuracy of ±0.14 % of the full-scale range. The pressure is recorded by a computer using a Cyber Research CYRDAS 1602 A/D Card, which is a 12 bit A/D having a full-scale range of 0–10 V.

The images recorded by the camera were gray-scale images, which were digitally converted to black and white in order to determine the saturation of air, the average position of the air and the fractal dimension of the invading fluid. This image conversion was performed by choosing a gray-scale threshold above which all pixels were converted to white (air), and below which all pixels were converted to black (water and glass). The threshold was chosen by visual inspection to optimize the accuracy of the air and water occupation of the cell in the final black and white image.

Consistent lighting irregularities, such as glare, will cause errors in the above "thresholding" process. In an attempt to remove this error, an image of the flow cell prior to the air injection was also converted to a black and white image; this basis image was then subtracted from the subsequent images. However, since lighting irregularities varied during the course of an experiment, the associated error was somewhat different for each picture, so that not all of the "error" could be removed by merely subtracting the basis image. A number

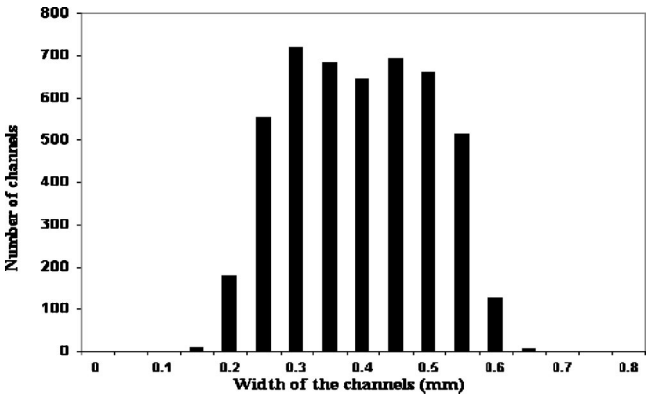

FIG. 3. Number distribution of channels in the flow cell.

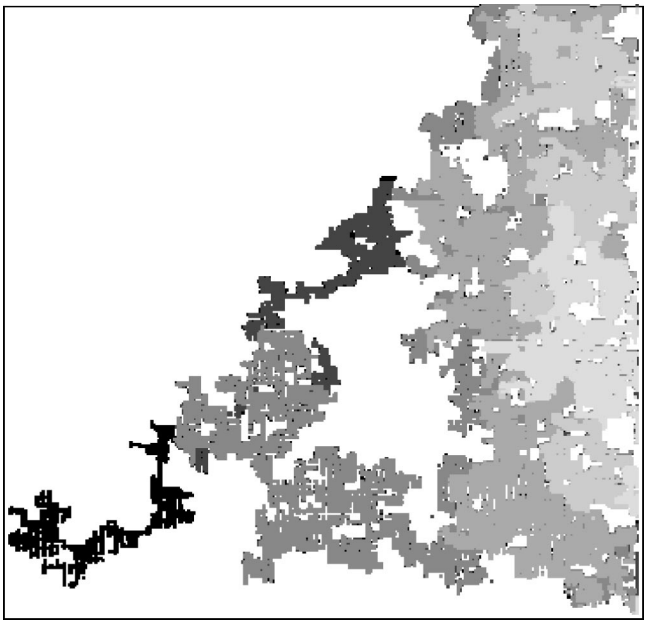

FIG. 4. Digitally converted photographs of the experiment where air was injected into the water saturated flow cell, shown in Fig. 1. For this flow, the capillary number is $N_c=8\times10^{-9}$. The different shades of gray represent different time intervals, from the lightest gray (earliest times) near the inlet at the far right center of the pattern to black (latest times) near breakthrough at the lower left-hand side. At a number of locations, some of the darker gray (later time flows) shows at the edges of lighter gray regions; most, if not all, of this is due to difficulties in the digital conversion and then overlapping the different photographic images taken at different times.

of small, slightly-below-threshold regions that were clearly not part of the injected air were not removed by the subtraction of the basis image. An algorithm was created to systematically remove these erroneous regions: a small box was inscribed around each white pixel; if no white pixels were found on the perimeter of this box, which was between 6 and 10 pixels wide, then the pixel was separated from the injected air and considered to be in one of the erroneous regions. Visual comparisons were used to verify this additional subtraction process. Once the gray-scale images were digitally converted to black and white images, the saturation of air, the average position of the air, and the fractal dimension were calculated.

B. Experimental results

Figure 4 shows the flow pattern at a very small injection rate, $q=0.002$ ml/min which corresponds to a capillary number of $N_c=8\times10^{-9}$. At this small capillary number, a capillary fingering pattern is expected; and, indeed, the pattern is characteristic of capillary fingering. The avalanche structure and the trapping, both characteristic of capillary fingering, are clearly evident. The lightest gray scale represents a time interval that would include a number of avalanches of injected air near the inlet. The black scale represents the final avalanche going to breakthrough. The darkest gray scale primarily represents one avalanche near the middle of the pat-

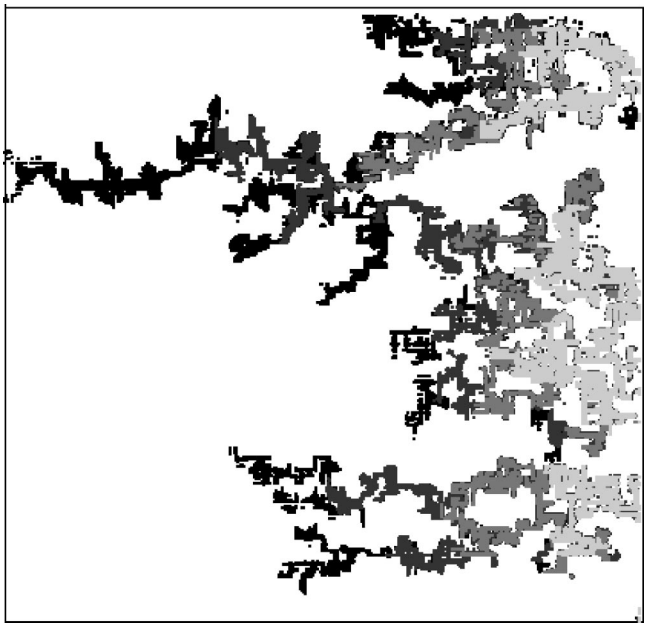

FIG. 5. Digitally converted photographs of the experiment where air was injected into the water saturated flow cell. For this flow, the capillary number is $N_c = 2 \times 10^{-5}$, so that the flow velocity is two thousand times larger than that in Fig. 4. Again, the different shades of gray represent different time intervals, from the lightest gray near the inlet at the far right center of the pattern to black near breakthrough at the upper left-hand side. As with Fig. 4, because of difficulties with reaching the threshold, some of the darker gray (later time flows) shows at the edges of lighter gray regions.

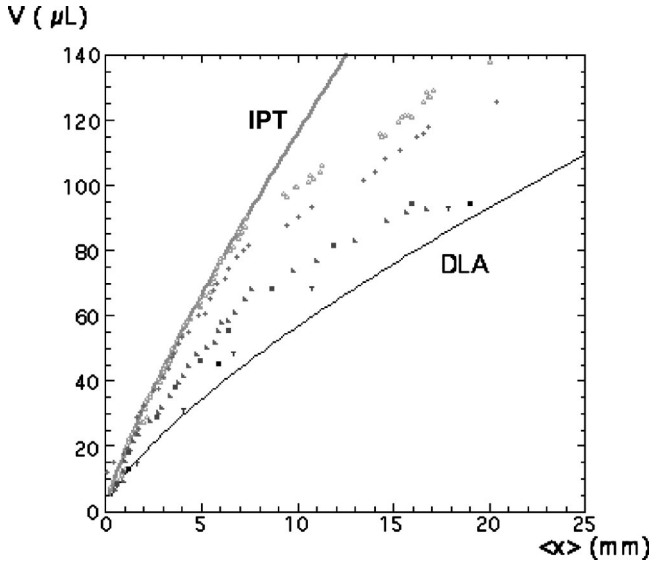

FIG. 6. Volume of air injected into the flow cell as a function of the average position of injected air, as determined from the photographs at a series of times, for a range of capillary numbers ($N_c = 2 \times 10^{-8}$, Δ; $N_c = 8 \times 10^{-8}$, ♦; $N_c = 4 \times 10^{-7}$, ▶; $N_c = 2 \times 10^{-6}$, ■; $N_c = 4 \times 10^{-6}$ ▼; and $N_c = 1.6 \times 10^{-5}$, ●). The solid gray line shows the IPT behavior as determined from a fit to the early time $N_c = 2 \times 10^{-8}$ data, using the correct fractal dimension for IPT, $D_f = 1.82$. The solid black line mimics the curvature of the DLA dependence with the DLA fractal dimension, $D_f = 1.714$.

tern. It should be noted that almost all the regions that are trapped during the time interval represented by one gray scale are not invaded by later (i.e., darker gray) flows. There are a very few (approximately four) regions which appear to be trapped during the times represented by the next-to-the-lightest gray scale but which are invaded during the next time (next darker gray scale) interval. This may occur because there could be a path out of the apparently trapped region, which was masked during the process of converting the photographic image to black and white; it also may represent a deviation from IPT because IPT is only exact at zero capillary number.

Figure 5 shows one of these time-resolved gray-scale patterns for a capillary number that is three orders of magnitude larger, $N_c = 2 \times 10^{-5}$, than the flow in Fig. 4. Clearly, there are significant qualitative differences between the flow patterns in Figs. 4 and 5. Although Fig. 4 exhibits characteristic capillary fingering, Fig. 5 exhibits viscous fingering, especially at the later times. Although there are a number of trapped regions, most prevalent at earlier times, there is little evidence of the avalanche structure where the flow initiates from a seed and then "bursts" into a region which is nearly as wide as it is long. On the other hand, all viscous fingers across a pattern tend to grow towards the outlet with the longer fingers growing the most. That is clearly present in Fig. 5 where in the last time interval (black region) a number of fingers all across the pattern are growing towards the outlet, with the longest finger growing the most. It seems apparent that during the earliest times, there is definite evidence of trapping and some evidence of avalanche structure; but this invasion percolation with trapping behavior has disappeared at the latest times, which are entirely consistent with viscous fingering.

In addition to presenting these figures, we have analyzed the photographs for a range of capillary numbers to determine fractal dimensions of the near-breakthrough patterns by box counting; also we have analyzed the photographs at consecutives times to determine the volume of air injected as a function of time, $V(t)$, and the average position of the injected air (as determined from the area in the photographs), $\langle x \rangle_t$. The box counting determines an average fractal dimension of the near-breakthrough patterns. The values of fractal dimension determined in this way are approximately correct, $D_f \approx 1.7 \pm 0.2$; unfortunately, for these small systems, the accuracy is not sufficient to distinguish between IPT and DLA.

However, plotting volume of air injected, V, vs average position of injected air, $\langle x \rangle$, does provide convincing evidence of the crossover from these experiments as it does with the modeling results in Fig. 8. The plot of V vs $\langle x \rangle$ as determined from the experiments is shown in Fig. 6. The early-time dependence of the smallest capillary number data is well fit by

$$V = A \langle x \rangle^{D_f - 1}, \tag{4}$$

using the correct IPT fractal dimension, $D_f = 1.82$, where the value of A from the fit is $A = 17.47$; this curve is given by the gray line in the figure. As was observed with the modeling results, the early-time (small-size) data follows the IPT behavior and then breaks away at characteristic size (or time),

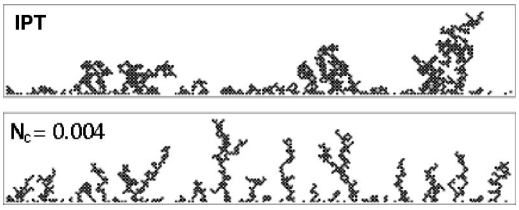

FIG. 7. For one particular realization, these figures show the pre-breakthrough patterns of injected fluid for the capillary numbers: (a) $N_c=0.0001$; (b) $N_c=0.004$.

which decreases with increasing capillary number. Unfortunately, the limitations of our photographic equipment severely limited the number of data points at the higher capillary numbers. However, the experiments clearly show the crossover from capillary fingering to viscous fingering at a characteristic size, which varies inversely with capillary number.

III. PORE LEVEL MODELING RESULTS

We have developed a pore-level model that includes both capillary and viscous forces in a two-dimensional model where pore bodies of volume ℓ^3 are located at the sites of a diamond lattice and are connected by throats of length ℓ and randomly chosen cross-sectional area varying uniformly from 0 to ℓ^2. The capillary number and viscosity ratio are determined from input values of the viscosities, surface tension, and net injection velocity. This model has been quantitatively validated in the limits of zero injection velocity (the IPWt limit) and in the limit of zero viscosity ratio and zero capillary forces (the DLA limit)[5]. Although this pore-level model is very comparable to other pore-level models in the literature [28,29,40–46], it is somewhat more flexible because both the pore throats and pore bodies have finite volume. Details of our model were described in earlier papers [5,47]; in the latter paper, we found a crossover from capillary fingering (IPT-like) to compact or Euclidean behavior as capillary number was increased for two fluids of equal viscosity, (viscosity ratio, $M=1$) so that capillary forces dominated the fingering.

Qualitatively, this is similar to the crossover from IPT-like flows to DLA-like flows discovered by Fernandez *et al.*; for zero viscosity ratio and finite capillary number, their smaller flows exhibit capillary fingering (IPT-like) but then the larger flows (at later times) exhibit viscous fingering (DLA-like) [1,2]. We have used our standard pore-level model to study two-phase flows for small viscosity ratio ($M=10^{-4}$) and a range of capillary numbers. Because this model is more general than the Fernandez model which explicitly builds in the DLA, we are restricted to smaller systems sizes than those studied by Fernandez *et al.* By being more general, this pore-level model does not restrict the physical options in the post-crossover flow; that is, our model will enable us to study the effect of larger viscosity ratios.

As shown in Figs. 7(a) and 7(b), we inject the low viscosity immiscible fluid along one side (the bottom of width W) of our rectangular porous medium of length $L=30$ pore bodies and width $W=180$ pore bodies. To improve statistics and avoid problems encountered with finger coarsening in long-narrow systems, we studied the flows in short-wide systems $(W>L)$ [24,48]. As with the experimental results in Figs. 4 and 5, these figures show the change from characteristic capillary fingering at the smaller capillary number to viscous fingering at the larger capillary number. Both cases shown in Fig. 7 are for the same realization of the porous medium, so that one can track specific changes as capillary number is increased.

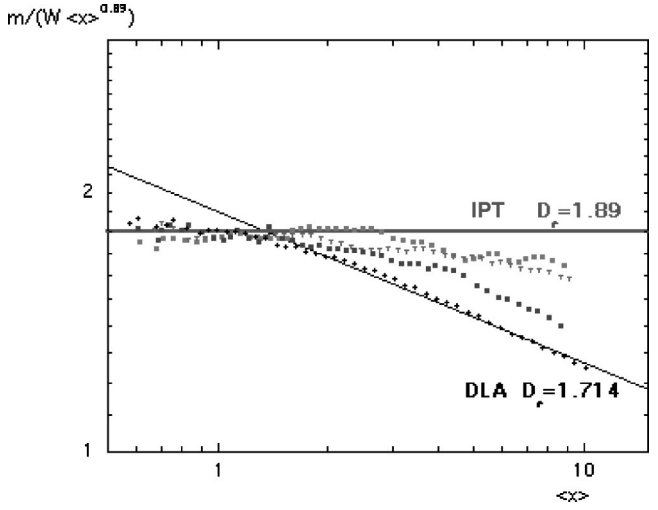

FIG. 8. Fractal character of the modeling results for mass, m, as a function of average position, $\langle x\rangle$, for a variety of capillary numbers $N_c=0.00025$ (○), $N_c=0.0005$ (▽), $N_c=0.001$ (⊞), and $N_c=0.002$ (◆). Length scales are in units of the lattice spacing. Distances are measured in units of $\ell/\sqrt{2}$; masses (equivalently volumes) are measured in units of ℓ^3.

At each time step, we determine the amount of injected fluid, m (proportional to the volume V), and the average position of this injected mass of fluid, $\langle x\rangle$, in the mean flow direction. For fractal patterns of injected fluid, the amount of injected fluid scales as a fractal power of the size of the pattern. For these systems, fractal scaling predicts that

$$m = AW\langle x\rangle^{D_f-1}, \tag{5}$$

where A is a constant sometimes called the lacunarity [10]. Available computer resources and the complexity of our code limit us to much smaller systems, $L\times W=50\times 150=7500$ pore bodies, than those studied by Fernandez in his less general, but computationally simpler model. For our small systems, direct plots of m vs $\langle x\rangle$ seem to provide more robust estimates of fractal dimension than do box-counting methods [24]. Figure 8 shows a plot of $m/(W\langle x\rangle^{0.89})$, which should be a straight line for capillary fingering, but which should decrease for viscous fingering like $A'\langle x\rangle^{-0.176}$, where the power is the difference between the DLA and IPT fractal dimensions [49]. The results for the smallest capillary number track the horizontal line and then break away at a moderately large size. Increasing the capillary number causes a decrease in the characteristic size at which the data break away from the horizontal IPT behavior towards the decreasing DLA-like

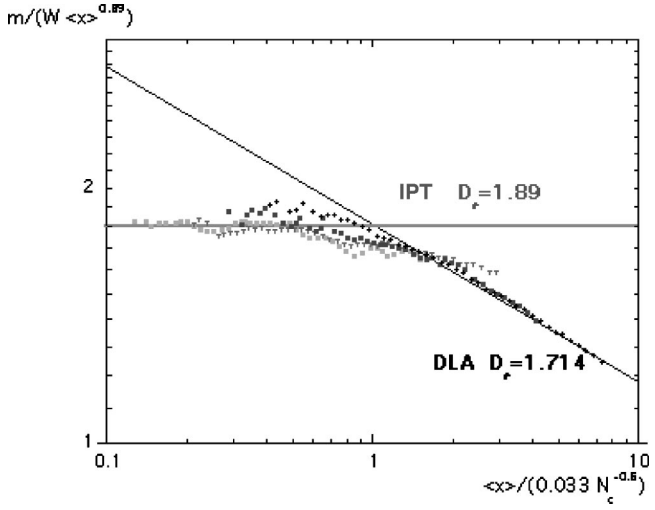

FIG. 9. $m/(W\langle x\rangle^{0.89})$ vs the scaled "average size" $u=\langle x\rangle/\Lambda_c$ for a variety of capillary numbers $N_c=0.00025$ (○), $N_c=0.0005$ (▽), $N_c=0.001$ (⊞), and $N_c=0.002$ (◆).

behavior. Fernandez *et al.* predicted that this characteristic size should have the form given in Eq. (2) [1]. Therefore, the mass of injected fluid should scale as

$$m = W\langle x\rangle^{0.89}\mathfrak{I}(\langle x\rangle/\Lambda_c), \tag{6}$$

where $\mathfrak{I}(u)$ is an unknown function of the average size in units of the characteristic length

$$\Lambda_c = 0.033N_c^{-0.6}. \tag{7}$$

The constant 0.033 was chosen so that the crossover would occur for $\langle x\rangle \approx \Lambda_c$.

The fractal scaling of the mass of injected fluid in terms of the scaled size is shown in Fig. 9. If the predictions of Eqs. (6) and (7) are valid, the data in Fig. 8 for $m/(W\langle x\rangle^{0.89})$ should collapse to one curve $\mathfrak{I}(u)$ when plotted vs the scaled length $u=x/\Lambda_c$. Figure 9 shows that this characteristic length does indeed collapse the data to one universal curve. It should be emphasized that this collapse is the result of the predicted power law behavior of Eq. (7); the constant 0.033 has no effect upon the collapse and only serves to shift the crossover to $u \simeq 1$.

IV. CONCLUSIONS

Our flow cell experiments clearly demonstrate the crossover from capillary fingering to viscous fingering as the capillary number is increased. The flow patterns Figs. 4 and 5 show the characteristic flows associated with capillary fingering and viscous fingering, respectively. More directly in Fig. 6, the volume of the injected air initially scales with its average position as predicted by IPT, but then crosses over to DLA-like behavior at a characteristic length which decreases as capillary number increases.

In agreement with experiment, simulations, using our standard pore-level model, also support the predicted IPT-to-DLA crossover; i.e., these simulations show the same crossover from IPT behavior for small sizes to DLA behavior for larger sizes at a characteristic length which decreases with increasing capillary number. Furthermore, the predicted power-law behavior for the characteristic length, Eq. (2), does collapse the simulation data to a single curve, which indicates that this scaling length correctly represents the capillary number dependence of the crossover.

ACKNOWLEDGMENTS

This work was supported by of the U. S. Department of Energy, Office of Fossil Energy. C.J. was supported by the NETL/University Partnership Program.

[1] J. F. Fernandez, R. Rangel, and J. Rivero, Phys. Rev. Lett. **67**, 2958 (1991).
[2] R. Rangel and J. Rivero, Physica A **191**, 253 (1992).
[3] P. Meakin, Physica A **173**, 305 (1991).
[4] D. S. Stauffer, *Introduction to Percolation Theory* (Taylor and Francis, Philadelphia, 1985).
[5] M. Ferer, G. S. Bromhal, and D. H. Smith, Physica A **319**, 11 (2003).
[6] R. Chandler, *et al.*, J. Fluid Mech. **119**, 249 (1982).
[7] D. Wilkinson and J. F. Willemsen, J. Phys. A **16**, 3365 (1983).
[8] D. Wilkinson, Phys. Rev. A **34**, 1380 (1986).
[9] M. Sahimi, *Flow & Transport in Porous Media & Fractured Rock From Classical Models to Modern Approaches* (VCH Verlagsgesellschaft, Germany, 1994).
[10] P. Meakin, *Fractals, Scaling, and Growth Far from Equilibrium* (Cambridge University Press, Cambridge, England, 1998).
[11] A. P. Sheppard, *et al.*, J. Phys. A **323**, L521 (1999).
[12] J. Feder, *Fractals* (Plenum, New York, 1988).
[13] T. Vicsek, *Fractal Growth Phenomena* (World Scientific, Singapore, 1989).
[14] S. Roux and E. Guyon, J. Phys. A **22**, 3693 (1989).
[15] L. Furuberg *et al.*, Phys. Rev. Lett. **61**, 2117 (1988).
[16] M. Ferer, G. S. Bromhal, and D. H. Smith, Physica A **311**, 5 (2002).
[17] A. Birovljev *et al.*, Phys. Rev. Lett. **67**, 584 (1991).
[18] V. Frette *et al.*, Phys. Rev. Lett. **68**, 3164 (1992).
[19] M. Rosso, J. F. Gouyet, and B. Sapoval, Phys. Rev. Lett. **57**, 3195 (1986).
[20] A. B. Dixit *et al.*, SPERE **2**, 25 (1999).
[21] M. J. Blunt, Curr. Opin. Colloid Interface Sci. **6**, 197 (2001).
[22] M. Cieplak and M. O. Robbins, Phys. Rev. B **41**, 11 508 (1990).
[23] M. M. Dias and D. Wilkinson, J. Phys. A **19**, 3131 (1986).
[24] M. Ferer, G. S. Brohmal, and D. H. Smith, Physica A **334**, 22 (2004).
[25] T. A. J. Witten and L. M. Sander, Phys. Rev. Lett. **47**, 1400 (1981).

[26] T. C. Halsey, Phys. Today **53**(11), 36 (2000).
[27] L. Paterson, Phys. Rev. Lett. **52**, 1621 (1984).
[28] R. Lenormand, E. Touboul, and C. Zarcone, J. Fluid Mech. **189**, 165 (1988).
[29] M. Blunt and P. King, Phys. Rev. A **42**, 4780 (1990).
[30] J. Nittmann, G. Daccord, and H. E. Stanley, Nature (London) **314**, 141 (1985).
[31] G. Daccord, J. Nittmann, and H. E. Stanley, Phys. Rev. Lett. **56**, 336 (1986).
[32] M. Ferer *et al.*, Phys. Rev. A **45**, R6973 (1992).
[33] J.-D. Chen and D. Wilkinson, Phys. Rev. Lett. **55**, 1892 (1985).
[34] M. Ferer and D. H. Smith, Phys. Rev. E **49**, 4114 (1994).
[35] M. Ferer *et al.*, AIChE J. **49**, 749 (1995).
[36] M. Ferer, J. Gump, and D. H. Smith, Phys. Rev. E **53**, 2502 (1996).
[37] P. Meakin, *et al.*, Phys. Rev. A **35**, 5233 (1987).
[38] P. Meakin and L. M. Sander, Phys. Rev. Lett. **54**, 2053 (1985).
[39] D. H. Smith *et al.*, in *2002 Fluid Engineering Summer Meeting*, Montreal, Canada, ASME, 2002.
[40] H. Siddiqui and M. Sahimi, Chem. Eng. Sci. **45**, 163 (1990).
[41] S. C. van der Marck, T. Matsuura, and J. Glas, Phys. Rev. E **56**, 5675 (1997).
[42] E. Aker, thesis, University of Oslo, 1996. Available at www.fys.uio.no/~eaker/thesis/thesis.html
[43] E. Aker *et al.*, Transp. Porous Media **32**, 163 (1998).
[44] E. Aker, K. Jorgen-Maloy, and A. Hansen, Phys. Rev. E **58**, 2217 (1998).
[45] E. Aker, K. Jorgen-Maloy, and A. Hansen, Phys. Rev. E **61**, 2936 (2000).
[46] G. Pereira, Phys. Rev. E **59**, 4229 (1999).
[47] M. Ferer, G. S. Bromhal, and D. H. Smith, Phys. Rev. E **67**, 051601 (2003).
[48] S. A. Curtis and J. V. Maher, Phys. Rev. Lett. **63**, 2729 (1989).
[49] This reflects the differences between the IPT and DLA fractal dimensions (1.89 and 1.714, respectively) used in our paper.